Electronic Supplementary Material (ESI) for Journal of Materials Chemistry A.

Supplemental information

Persulfate salt as an oxidizer for biocidal energetic nano-thermites

Wenbo Zhou,[a] Jeffery B. Delisio,[b] Xiangyu Li,[c] Lu Liu[b] and Michael R. Zachariah*[a,b]

[a] *Department of Chemical and Biomolecular Engineering, University of Maryland, College Park, Maryland, 20742, U.S.A.*
[b] *Department of Chemistry and Biochemistry, University of Maryland, College Park, Maryland, 20742, U.S.A. E-mail: mrz@umd.edu*
[c] *Nanjing University of Science and Technology, Nanjing, Jiangsu 210094, China*

Table S1 List of bond energies of M-O in peroxy salts (M=Cl, Br, I, Mn, Cr, S) as well as oxygen contents in peroxy salts and relevant aluminum-based, stoichiometrically mixed thermite composites.

Thermite[a]	BDE (kJ/mol)[b]	Oxygen content in salt (%)	Oxygen content in thermite (%)
3CuO+2Al	287 (Cu-O)[1]	20	16
Fe_2O_3+2Al	407 (Fe-O)[1]	30	22
Bi_2O_3+2Al	337 (Bi-O)[1]	10	9
$3Ag_2O$+2Al	221 (Ag-O)[1]	7	6
$3I_2O_5$+10Al	184 (I-O)[2]	24	19
$3KIO_4$+8Al	184 (I-O)[2]	28	21
$3KBrO_4$+8Al	235 (Br-O)[2]	35	25
$3KClO_4$+8Al	269 (Cl-O)[2]	46	30
$3KMnO_4$+8Al	406 (Mn-O)[2]	41	28
$3K_2Cr_2O_7$+14Al	423 (Cr-O)[2]	38	27
3K2S2O_8+16Al	142 (O-O)[3]	47	31
$3K_2SO_4$+8Al	365 (S-O)[3]	37	26

Note:

[a] Fuels and oxidizers mixed in a stoichiometric ratio that presumably all the oxygens in oxidizers were converted into alumina in the product.

[b] Bond dissociation energy (BDE) data were based on measurement of the standard dissociation enthalpies of M-O diatomic species at 25 ˚C by either spectroscopic or thermochemical methods. BDE data of Cr-O was calculated at -273 ˚C.

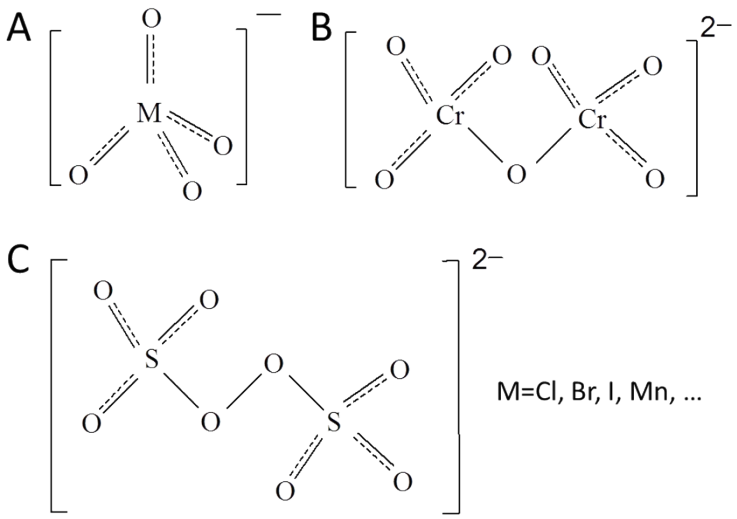

Figure S1 Molecular structures of three types of peroxy salt anions. (A) includes perchlorate (ClO_4^-), perbromate (BrO_4^-), periodate (IO_4^-), permanganate (MnO_4^-). (B) is dichromate ($Cr_2O_7^{2-}$). (C) is persulfate ($S_2O_8^{2-}$).

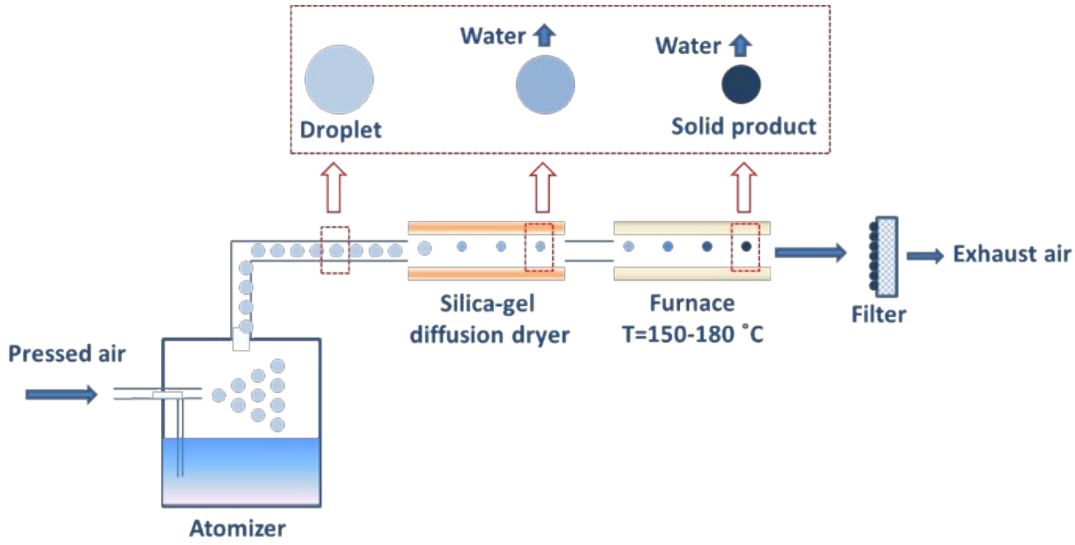

Figure S2 Spray-drying process of preparing nano-oxysalts.

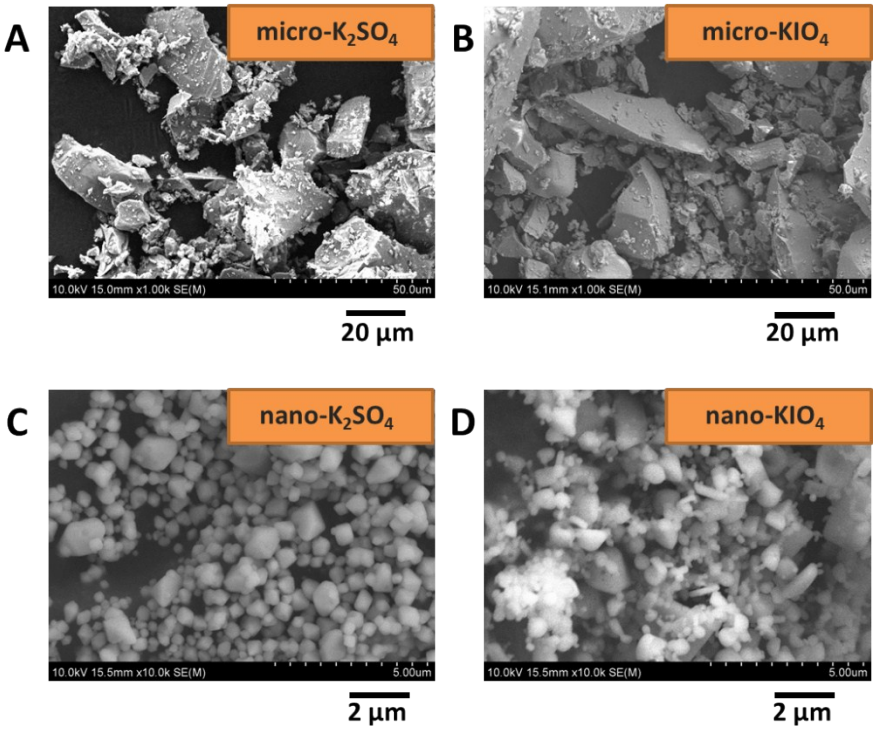

Figure S3 SEM images of as-received micro-sized K_2SO_4 (A) and KIO_4 (B) powders, as well as SEM images of nano-sized K_2SO_4 (C) and KIO_4 (D) prepared by spray-drying.

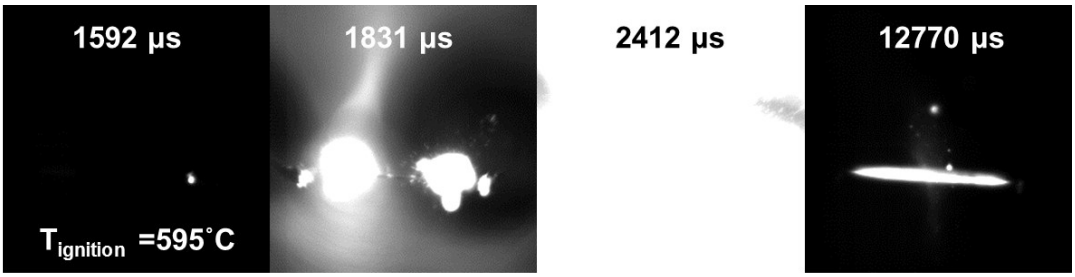

Figure S4 High speed imaging of the wire burning tests for nano-Al/$K_2S_2O_8$ in Ar. The pulse lasting time for each snapshot and the ignition temperatures are denoted. The heating rate is ~4×10^5 ˚C/s.

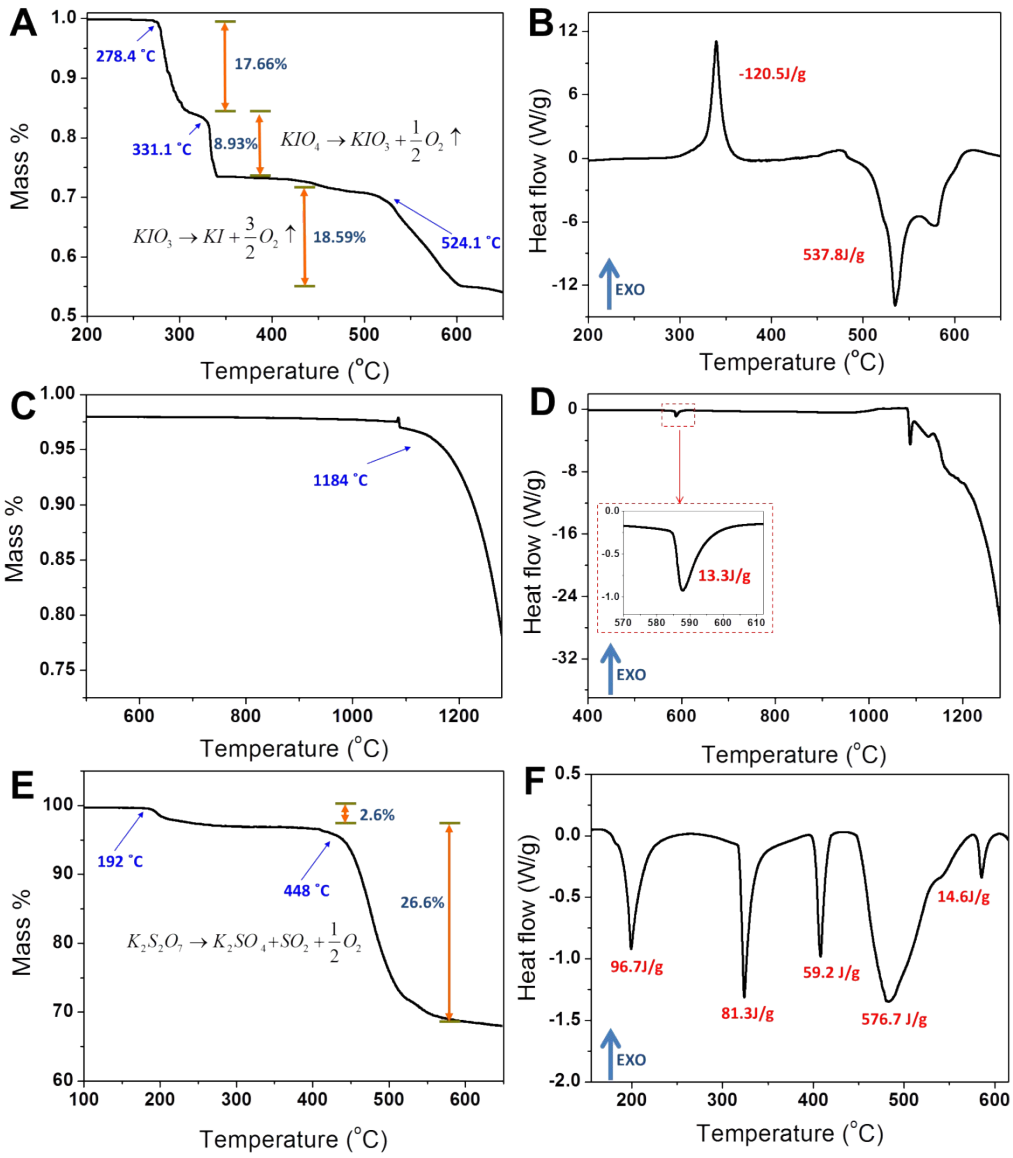

Figure S5 TG and DSC profiles of nano-KIO_4 (A and B), nano-K_2SO_4 (C and D), and $K_2S_2O_7$ (E and F). The heating rate is 10 ˚C/min. The initial mass reduction in $K_2S_2O_7$ pertains to a water evaporation step (2.6% mass loss) (E), with an endothermic enthalpy change of 96.7 J/g (F).

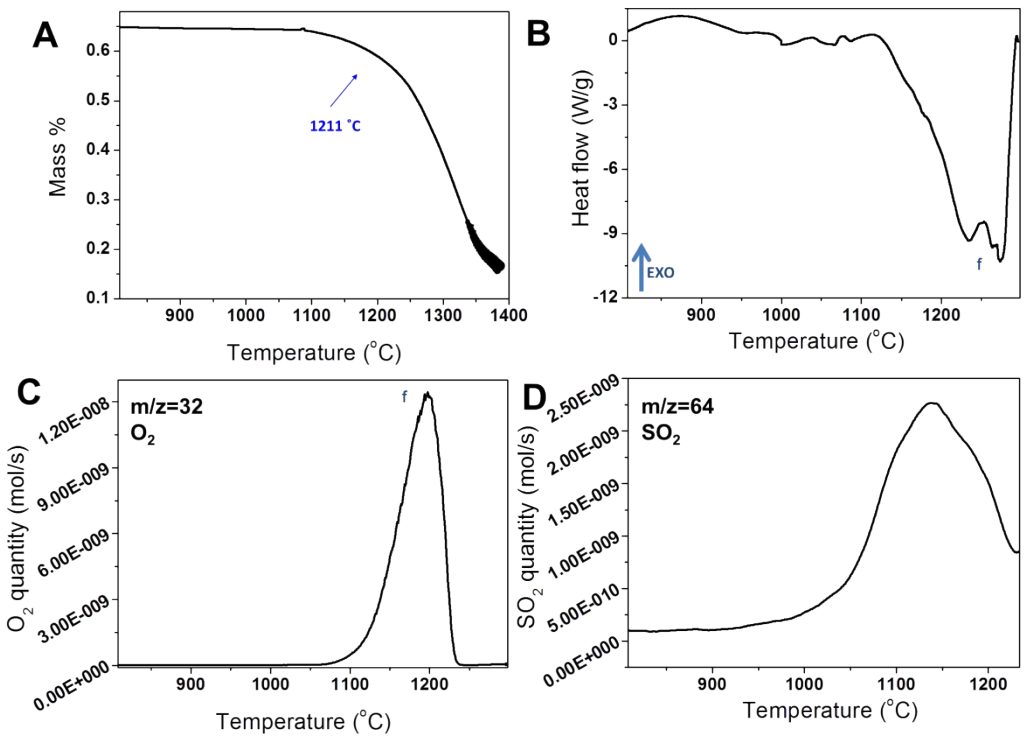

Figure S6 TG (A), DSC (B) and MS for O_2 (C, m/z=32) and SO_2 (D, m/z=64) profiles of nano-$K_2S_2O_8$ in the high temperature range starting from 800 ˚C.

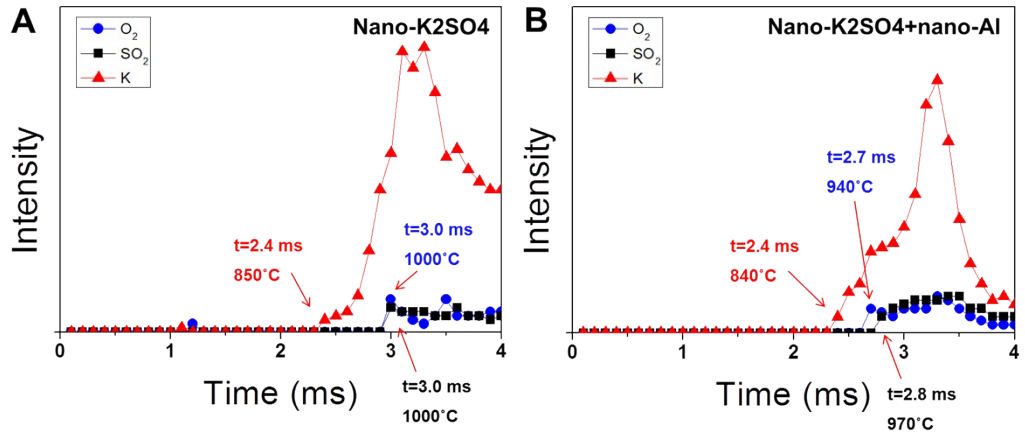

Figure S7 TOF-MS temporal profiles of molecular species O_2, SO_2 and K during ultrafast thermal decomposition of nano-K_2SO_4 (A) and thermite reaction involving nano-Al and nano-K_2SO_4 (B). Measured data at each time point are denoted as circle, square and triangle remarks for O_2, SO_2 and K species, respectively. The starting times and temperatures for different MS peaks are shown.

Thermal analyses of the decomposition of nano-$K_2S_2O_8$:

1. Peak A and B:

The decomposition transition from $K_2S_2O_8$ to $K_2S_2O_7$ was observed in two mass reduction sub-steps, with an initial major mass reduction of 5.4% starting at 270 ˚C followed by a second minor mass reduction of 0.4% at 312 ˚C (Fig. 4A). MS results show that this two-step mass reduction is due to the generation of bimodal oxygen peaks at 270 ˚C and 310 ˚C (Fig. 4C). The appearance of these two subsequent sub-steps implies the possible inhomogeneity within nano-$K_2S_2O_8$, which is proposed to be due to the difference between surface and bulk of particles. While the nature of the reasons for these two steps is unclear, the mass reduction and O_2 emergence is quantitatively consistent with this transition.

DSC results further show that these two mass reduction sub-steps correspond to an initial exothermic peak A (T=273 ˚C) and a subsequent endothermic peak B (T=313 ˚C) respectively (Fig. 4B). Peak A represents the major decomposition step, yielding a heat of reaction (ΔH) of -288 J/g. In contrast, peak B is endothermic (ΔH=64.2 J/g). To understand this endotherm, $K_2S_2O_7$ was tested as a control, which was prepared after heating nano-$K_2S_2O_8$ to 380 ˚C as confirmed by XRD (Fig. 5). Fig. S5F shows that most of the endothermic peaks of $K_2S_2O_7$ are consistent with those of nano-$K_2S_2O_8$, except for the peak at 310 ˚C that shows a higher endothermic enthalpy change (81.3 J/g) than that of nano-$K_2S_2O_8$ at the same temperature (64.2 J/g, see Fig. 4B). This peak represents the phase change of $K_2S_2O_7$. Hence, the endothermic peak B of nano-$K_2S_2O_8$ (64.2 J/g, see Fig. 4B) is, in fact, a combination of an endothermic phase change peak of generated $K_2S_2O_7$ (81.3 J/g) and a small exothermic O_2 release peak of nano-$K_2S_2O_8$ (64.2 J/g-81.3 J/g = -17.1 J/g, see Table 2). Further combining the exotherms of the two O_2 release peaks gives the total exothermic enthalpy change of the decomposition reaction of $K_2S_2O_8$ to $K_2S_2O_7$ as -305.1 J/g (Table 2).

2. Peak C, D and E:

The endotherm at 405 ˚C (peak C, see Fig. 4B) corresponds to the melting of $K_2S_2O_7$ as was visually observed. The heat of melting was measured to be 61.8 J/g, which is confirmed by the melting enthalpy change of pure $K_2S_2O_7$ (59.2 J/g) in Fig. S6F. Further increases in temperature to 442 ˚C result in a large mass reduction step (29.8%) corresponding to the decomposition of $K_2S_2O_7$ to K_2SO_4 (Fig. 4A). DSC results show that this step corresponds to the endothermic peak D at 453 ˚C (Fig. 4B), with a heat of reaction of 570.0 J/g, which is similar to the value (576.7 J/g) measured from pure $K_2S_2O_7$ in Fig. S5F. The small endothermic peak E at 582 ˚C, with an enthalpy change of 13.3 J/g, has no mass change associated with it, suggesting a phase change in K_2SO_4, which is confirmed by both heating profiles of $K_2S_2O_7$ (Fig. S5F) and K_2SO_4 (Fig. S5D).

3. Peak F:

The final decomposition step F started at 1211 ˚C (Fig. S6A) and lasted over a wide temperature range exceeding the upper limit of our TG temperature capabilities. Thermogravimetric analysis of nano-K_2SO_4 was also conducted, which shows a similar onset temperature for decomposition at 1184 ˚C (Fig. S5C). This step of K_2SO_4 decomposition possesses the largest endothermic peak (ΔH=5463 J/g) (Fig. S6B). Despite the fact that the final products were unknown, this result, at the very least, demonstrates that K_2SO_4 is much more difficult to decompose than $K_2S_2O_8$.

Side reaction of O_2 and SO_2 in the micro-capillary:

In step D, a small oxygen signal at 455 ˚C (Fig. 4C) is seen in addition to SO_2 at 460 ˚C (Fig. 4D) suggesting that the decomposition of $K_2S_2O_7$ generates O_2, SO_2, and K_2SO_4:

$$K_2S_2O_7 \rightarrow K_2SO_4 + SO_2 + \frac{1}{2}O_2 \quad \text{(S1)}$$

The net mole fractions of O_2 and SO_2 detected from MS in this step are 6.7×10^{-9} and 5.2×10^{-10}, respectively, which are much smaller than theoretical values (7.1×10^{-8} for O_2 and 1.4×10^{-7} for SO_2) based on the original dose of samples (Fig. 4A). The likely reason for the discrepancy is that SO_2, as it passes through the much cooler micro-capillary (around 300 ˚C), undergoes a reaction yielding sulfuric acid:

$$SO_2 + \frac{1}{2}O_2 + H_2O \rightarrow H_2SO_4 \quad \text{(S2)}$$

Considering that the measured intensity of background H_2O signal is around two orders of magnitude higher than that of the generated O_2 and SO_2 in the MS, it is reasonable to estimate that the molar ratio of SO_2:O_2:H_2O is 1:1:100. Using the on-line Chemical Equilibrium with Applications (CEA) code from NASA[4], the converted proportions of these reactants, after achieving the reaction equilibrium at 300 ˚C, can be obtained. The result shows that most SO_2 and O_2 were reacted and only 0.4% O_2 and 0.0003% SO_2 remained, thus supporting the proposed explanation of low intensities of O_2 and SO_2 signal in step D. H_2SO_4 was not apparent in the MS results. This is most likely due to H_2SO_4 adsorbing to the inner wall of micro-capillary.

At higher temperatures >1100 ˚C (step F), weak SO_2 and O_2 MS signals were also detected which correspond to a net mole fraction of 1.1×10^{-8} for O_2 and 4.4×10^{-9} for SO_2, respectively. Recalculation of the chemical equilibrium in e.q S2 was conducted. In this case, a higher reaction temperature of 1100 ˚C and a similar molar ratio of SO_2:O_2:H_2O of 1:1:100 were

employed. The result shows that 0.5% of both SO_2 and O_2 were retained, indicating that most of these gases had reacted before entering the MS.

References:

1 Y. R. Luo, *Comprehensive handbook of chemical bond energies*, CRC Press, Boca Raton, FL, 2007.

2 B. D. Darwent, *Bond dissociation energies in simple molecules*, Nat. Stand. Ref. Data Ser., Nat. Bur. Stand. (U.S.), 1970, **31**, 1-52.

3 R. T. Sanderson, *Chemical bonds and bond energy*, Academic Press, New York, London, 1971.

4 http://www.grc.nasa.gov/WWW/CEAWeb/.